Seasonal and developmental stage changes in exudate carbohydrate content shapes the kelp microbiome

Chance J. English[1], Meenakshi Manoj[1], Keri Opalk[1], Craig A. Carlson[1]*

1. Marine Science Institute/Department of Ecology, Evolution and Marine Biology, University of California Santa Barbara, CA, USA

* Corresponding author: Chance J. English

Email: cje@ucsb.edu

(951) 286-8416

Key Words: microbiome, macroalgae, dissolved organic carbon, carbohydrates, planctomycetota, alginate, fucoidan

Author Contribution Statement

CJE and CAC conceptualized the research. CJE collected material for and ran the incubations. CJE, MM, and KO collected data and performed laboratory measurements. CJE, MM, KO, and CAC contributed to interpreting the results and writing/editing the manuscript. CAC acquired funding for the research.

Abstract

Photoautotrophs release a large amount of their fixed carbon as exudates, which shapes their immediate environment, including the composition of their microbiome. Here we evaluated the microbiome and exudate composition of *Macrocystis pyrifera* (giant kelp), a globally distributed foundation species, in response to seasonal nutrient availability and developmental stage. We combine 16S rRNA amplicon analysis of the giant kelp microbiome with carbohydrate monomer analysis of kelp exudates to examine microbe-exudate relationships. We found significant differences in the microbiome and exudate composition between seasons and developmental stages of giant kelp. Higher tissue-nitrogen content in the spring coincided with elevated amounts of glucosamine, a nitrogen-containing sugar, in giant kelp exudates, while senescence led to the release of mannuronic acid, an alginate indicator. The release of glucosamine and fucose-rich exudates was correlated with an increase in the abundance of bacteria within the *Planctomycetota* phylum, whereas mannuronic acid-rich exudates coincided with an increase in the abundance of members of the Flavobacteria and Gammaproteobacteria lineages. We investigated putative carbohydrate-microbe relationships by isolating a member of the *Planctomycetota* phylum from the surface of giant kelp. We demonstrate that the growth of this isolate on fucoidan and *N*-acetyl glucosamine, but not alginate reflects the observed abundance of this clade in the kelp microbiome in response to variable carbohydrate exudation. This suggests a key role of kelp mucilage carbohydrate composition in structuring its microbiome as has been observed for other organisms such as corals and within the human gut.

Introduction

Primary producers such as plants and macroalgae have evolved in environments surrounded by microorganisms, and in many cases, associated microbes can improve the fitness and growth of the host through defense or nutrient acquisition [1–4]. A growing body of evidence indicates that autotrophic organisms regulate their microbiome by exuding metabolites that promote microorganism growth or inhibit the growth of pathogens [5, 6]. The exudate and host-microbe associations are dynamic and can vary in response to the host's developmental stage and abiotic stressors [7, 8]. Unraveling the relationship between host physiology, exudate composition, and the microbiome structure can provide a mechanistic understanding of the establishment and function of the microbiome of primary producers.

Carbohydrates, including simple sugars, disaccharides and complex polysaccharides are typically the dominant organic material exuded by primary producers [9, 10]. The active exudation of carbon-rich organic matter by organisms was originally proposed as an "overflow" mechanism that allowed photosynthesis to continue when light and nutrients needed for biosynthesis became uncoupled [11, 12]. More recently, it has been proposed that the exudation of carbohydrate-rich material can also serve to prevent the attachment of pathogens [5], promote the growth of beneficial microbial partners [8, 13] or aid in the transport of energy and nutrients to the organism [14]. The potential role of carbohydrate exudation in shaping microbiomes is evidenced in studies of corals that reveal significant correlations between the host's exuded mucus sugar content and the abundance of certain microbial taxa [15, 16]. The composition of exuded carbohydrates by

corals is species-specific [17, 18] and varies in response to abiotic factors such as temperature [15]. While these relationships are established for corals, the role of carbohydrate exudation in shaping the microbiome has yet to be evaluated for important foundation species such as kelps.

Kelp forests are critical marine habitats that occupy 43% of the world's coastline [19]. In addition to their contributions to biodiversity [20] and global economies [21], it is hypothesized that kelps contribute to carbon sequestration through the export of dissolved organic carbon (DOC) and detrital particulate carbon [22–24]. In this context, the decline of kelp forests [25] due to stressors such as ocean warming is a serious threat to ecosystem function, marine carbon cycling, and economies. This has prompted calls for large-scale intervention through natural kelp forest restoration [26] or aquaculture to offset these losses and increase current production yields [27]. Therefore, identifying and understanding the underlying factors for kelp health and resilience is of critical importance for monitoring, management, and restoration of these ecosystems, their services, and the economies dependent on kelp.

Decades of research have focused on understanding the impact of environmental factors such as light, nutrients, wave disturbance, and temperature on kelp growth [28–32]. In comparison, little is known about how the kelp microbiome affects kelp growth and resilience. Several studies demonstrate that kelp harbor a microbiome that is distinct from the surrounding seawater [33–35] and metagenomic analysis of kelp microbiomes suggest potential positive interactions between kelp and specific microbial lineages. Further, there are significant relationships between the physiological condition of kelp, its productivity,

92 and its microbiome [36, 37]. However, the underlying mechanisms between kelp
93 physiology and its microbiome composition are unresolved.
94 In this study, we aimed to understand how the composition of kelp exudates shapes
95 the microbiome of *Macrocystis pyrifera*, hereafter giant kelp. We hypothesized that abiotic
96 factors (nitrogen availability) and developmental stage would alter the chemical
97 composition of kelp exudates and that these altered chemical profiles would shape the
98 giant kelp microbiome. We tagged cohorts of giant kelp fronds in the summer and spring to
99 track the development of the kelp microbiome across nutrient deplete and replete
100 conditions and developmental stages. Simultaneous measurements of exudate
101 carbohydrate composition and 16S rRNA gene analysis were employed to identify microbe-
102 exudate associations. We observed significant correlations between abundant microbial
103 taxa and the carbohydrate content of giant kelp exudates. To test some of these
104 associations, we isolated a member of the *Planctomycetota* phylum, a main kelp-
105 associated bacterial group. We demonstrate that its carbohydrate substrate preferences
106 reflect this bacterial clade's seasonal and developmental stage abundance patterns in the
107 kelp microbiome. This work suggests an important role for exuded carbohydrates in the
108 establishment of the kelp microbiome.
109
110 **Methods**
111 *Sampling, kelp blade age and developmental stage, and environmental variables*
112 Giant kelp blades were sampled from two tagged cohorts at Mohawk Reef (34º
113 23.6600' N, 119º 43.8000' W) in the Santa Barbara Channel, CA, USA in the summer of

2023 and spring of 2024. Age cohorts were established by tagging 100-200 fronds at a blade 2 m back from the growing tip (blade ~14 days of age). At intervals of 2-3 weeks, single blades from 6 random fronds were sampled to measure their tissue nitrogen (tissue-N), exudate carbohydrate composition and microbiome. Blades were collected in the morning (08:00-10:00) and transported to a near-shore laboratory, where they were incubated in 10 L acrylic tanks filled with filtered (0.2 μm) seawater. Incubations were started between 10:00-12:00 and maintained at *in situ* temperature using a temperature-controlled water bath for 6-9 hours. Light levels were adjusted every 2-3 hours, decreasing from saturating intensity (1140-1517 μmol photons m^{-2} s^{-1}) to darkness (0 μmol photons m^{-2} s^{-1}) to simulate the transition from day to night. Seawater DOC and hydrolyzable carbohydrate samples were taken at the beginning and end of each incubation, filtered through pre-combusted GF-75 (0.3μm nominal pore size). Following incubation, kelp blade tissue-N was sampled as a measure of nitrogen stress and developmental stage. For tissue-N analysis, giant kelp blades were cleaned of epibionts, dried at 60 ºC for three days and then ground to a fine powder before analysis with an Exeter Analytical CE-440 CHN/O/S elemental analyzer. The developmental stage of kelp blades was categorized as either “mature” or “senescent” if they were younger than or older than 50 days old, respectively [29].

Environmental conditions at Mohawk Reef during our study were evaluated using bottom temperature data collected by the Santa Barbara Channel Long-Term Ecological Research program [38]. Average daily temperature was calculated from submersible temperature loggers at Mohawk Reef. Nitrate concentrations were calculated from

temperature using an exponential "T2N" relationship derived from an inshore temperature and nitrate dataset [39] (Supplemental Figure. 1).

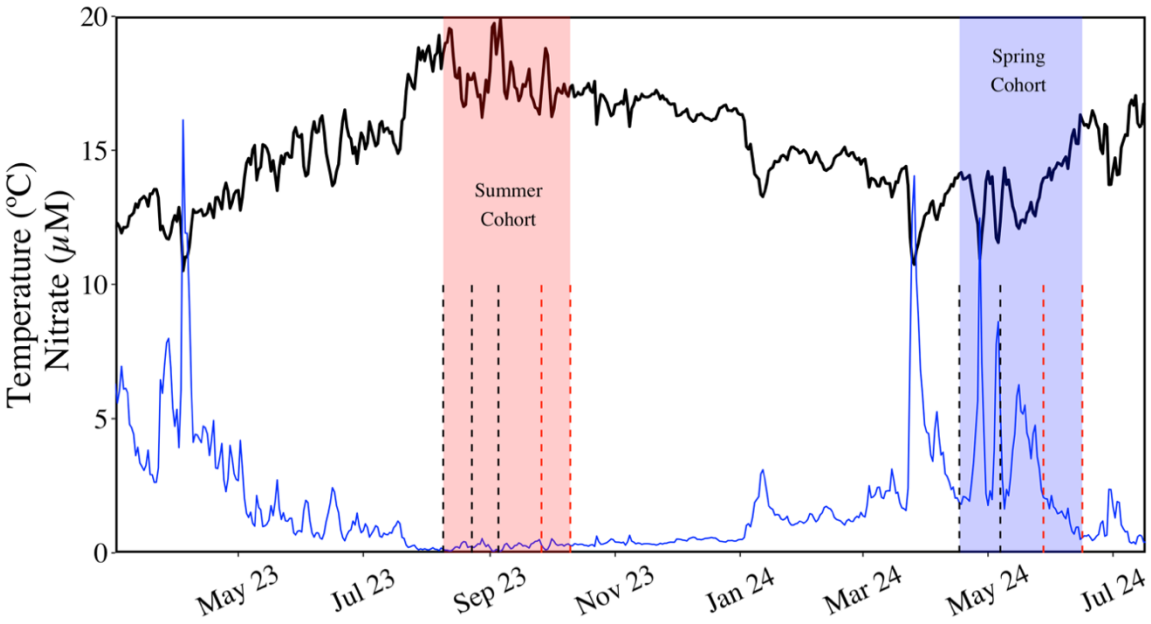

Figure 1. Mohawk Reef environmental conditions and sampling dates in this study. Daily average temperature (solid black line) and nitrate (solid blue line) concentrations between January 2023 and August 2024. Shaded red and blue regions show the sampling periods for the summer and spring cohorts used in this study, respectively. Vertical dashed lines extending from the x-axis mark the sampling dates within each cohort. The black and red color of the dashed lines indicate sampling of kelp that was in a mature (< 50 days) or senescent (> 50 days) development stage, respectively.

Exudate DOC, carbohydrate content and composition

DOC analysis was carried out following established protocols [40]. Briefly, duplicate DOC samples were taken from at beginning and end of each incubation, filtered through pre-combusted 25 mm GF-75 (0.3 µm) into pre-combusted 40 ml EPA vials with PTFE lined caps, acidified to pH < 3 with the addition of 60 µl of 4N HCl and analyzed using a Shimadzu TOC-V or TOC-L.

154 Dissolved carbohydrate samples were taken alongside DOC samples and stored
155 frozen at -20ºC. Exudate carbohydrate content was measured by high-performance anion
156 exchange chromatography with pulsed amperometric detection (HPAEC-PAD). We
157 followed established dialysis and HPAEC-PAD gradient specified by Engel and Händel
158 (2011). Briefly, samples were dialyzed using Spectra/Por 7 tubing (1000 Da) against
159 ultrapure water and then hydrolyzed in duplicate for 20 hours at 100°C in 0.4 M HCl then
160 neutralized under a flow of N_2 gas. Samples were run on a DIONEX ICS5000+ and sugars
161 were separated using a Carbopac PA10 column (4x250mm) with a Carbopac PA10 guard
162 column (4x50mm). Neutral and amino sugars were eluted with 18mM NaOH followed by
163 100mM NaOH/200mM Na-Acetate to elute acidic sugars. The system was calibrated using
164 a standard sugar mix containing fucose, rhamnose, arabinose, galactosamine,
165 glucosamine, galactose, glucose, mannose+xylose, galacturonic acid, glucuronic acid and
166 mannuronic acid. Linearity of the calibration curves were observed for concentrations
167 ranging from 10nM-1μM. In our dissolved carbohydrate samples, we observed glucose and
168 mannose+xylose contamination due to leaching from the Spectra/Por 7 dialysis tubing, so
169 these sugars were removed from subsequent analysis. Previous studies demonstrate
170 these sugars are not substantial components of carbohydrates released by brown
171 macroalgae [17, 42].
172 Principal component analysis was used to visualize changes in the composition of
173 hydrolyzable sugar monomers in giant kelp exudates. Sugars were normalized to molar
174 percentages (mole%) relative to other sugars. Statistical analysis of the differences in the
175 composition of the carbohydrates released by giant kelp between the two seasons and

176 developmental stages was evaluated by PERMANOVA on the scaled mole% of individual
177 sugar monomers.
178
179 *Microbiome DNA extraction, 16S rRNA gene sequencing & amplicon analysis*
180 Following their incubation, kelp blades were rinsed with 0.1 µm filter sterilized
181 seawater and sampled across the entire surface by scraping with sterile cotton-tip swabs
182 (Puritan®) for 30 seconds. Swabs were placed in sterile 2 ml cryogenic tubes and frozen at -
183 80 ºC. DNA samples were lysed in sucrose lysis buffer with 1% SDS and 0.2 mg mL^{-1}
184 proteinase-K at 37ºC for 30 minutes, then at 55ºC for 30 minutes. DNA was purified using
185 the phenol-chloroform method [43]. For amplification, we targeted the V4 region of the 16S
186 rRNA gene using the 515F-Y (5'-GTGYCAGCMGCCGCGGTAA-3') and 806RB (5'-
187 GGACTACNVGGGTWTCTAAT-3') primers with custom adaptors [44]. PCR was carried out
188 in reactions with 12.5 µL KAPA Robust Hotstart ReadyMix, 1uL each of the forward and
189 reverse primers, 2µL of bovine serum albumin, 6.5 µL of PCR-grade water and 2µL of
190 sample DNA and cycled for 3 minutes at 95 ºC, followed by 30 cycles of 30 seconds at 95
191 ºC, 30 seconds at 57 ºC and one minute at 72 ºC, ending with 10 minutes at 72 ºC. Four
192 negative controls (PCR-grade water) and two mock community samples were included in
193 the PCR run for quality control. Following PCR, amplified DNA was quantified (Qubit,
194 Thermo Fisher) and manually normalized by pooling equal nmol amounts of DNA from
195 each PCR reaction well. Pooled DNA was concentrated using Amicon Ultra 0.5mL 3K
196 centrifugal filters (Millipore). Non-target DNA bands were removed by gel extraction.

197 Samples were sequenced at the University of California, Davis DNA Technologies Core on
198 an Illumina MiSeq using PE250.

199 Demultiplexed raw sequence reads were processed using DADA2 (Callahan et al.,
200 2016; v1.16) in R. Forward and reverse reads were trimmed to 240 and 150 bp, respectively
201 and assigned taxonomy using the SILVA database (Quast et al., 2012; v138.1 with species).
202 Amplicons identified as mitochondria or chloroplasts were removed. Quality filtering of
203 chimeric sequences or sequences with ambiguous bases resulted in 4.4×10^6 sequences
204 from 54 samples. Samples had a read depth from 25,077 to 106,379 sequences, averaging
205 81,976 and were not rarefied for further analysis [47]. We analyzed differences in
206 microbially community composition on kelp blades by season (summer vs. spring) and
207 developmental stage (mature vs. senescent).

208 For multivariate analysis, singleton and doubleton amplicon reads were removed
209 and remaining amplicon sequence variants (ASVs) were converted to relative abundances
210 and normalized using a variance stabilizing transformation. For diversity metrics, singleton
211 and doubleton amplicons were not removed. Significant differences in the mean relative
212 abundances of amplicons by season and developmental stage were evaluated using the
213 "DEseq2" package in R [48]. Differentially abundant ASVs were those that displayed a log2
214 fold-change >1.5 between developmental stage or season and a significant false discovery
215 rate (FDR)-adjusted p-value (<= 0.01).

216 To identify relationships between the giant kelp microbiome and the exudate
217 carbohydrate composition we used Spearman's rank correlations and hierarchical
218 clustering of differentially abundant ASVs and the mole% of sugar monomers

219 simultaneously released by giant kelp blades. This clusters ASVs based on their degree of
220 correlation with the sugar content of kelp exudates and allowed us to identify positive or
221 negative microbe-carbohydrate relationships. Hierarchical clustering was arranged by
222 Euclidean distance using the *pheatmaps* package in R.
223
224 *Planctomycetota cultivation & growth on model carbohydrates*
225 We enriched and isolated a strain of *Planctomycetota* following the suggestions of
226 Lage & Bondoso (2012) and Wiegand et al., (2020) [49, 50]. Agar plates were prepared with
227 0.1 µm filtered seawater with 1% agar. Seawater was autoclaved with agar then
228 supplemented with 1ml l^{-1} vitamin solution (Biotin: 2 mg/L, Folic acid: 2 mg/L,
229 Pyridoxamine-HCl: 10 mg/L, Thiamine-HCl x $2H_2O$: 5 mg/L, Riboflavin: 5 mg/L, Nicotinic
230 acid: 5mg/L, D-ca-pantothenate: 5 mg/L, Cyanocobalamine: 0.1 mg/L, p-Aminobenzoic
231 acid: 5 mg/L, Lipoic acid: 5mg/L, KH_2PO_4: 900 mg/L) and 1ml l^{-1} trace metal solution (H_3BO_3:
232 2860 mg/L, $MnCl_2$ x $4H_2O$: 1810 mg/L, $FeCl_3$ x $6H_2O$: 316 mg/L, $ZnSO_4$ x $7H_2O$: 222 mg/L,
233 Na_2MoO_4 x $2H_2O$: 390 mg/L, $CuSO_4$ x 5 H_2O: 79 mg/L, $Co(NO_3)_2$ x $6H_2O$: 49 mg/L). For a
234 carbon and nitrogen source we added 10 ml of 5% *N*-acetyl glucosamine. To prevent fungal
235 growth and select for *Planctomycetota*, the medium was supplemented with 20 mg l^{-1} of
236 econazole nitrate, 200 mg l^{-1} ampicillin and 1 g l^{-1} streptomycin. Bacterial inoculum was
237 scraped from the surface of a giant kelp blade using a sterile swab for 30 seconds and
238 resuspended in sterile medium without agar. The cell suspension was filtered through a
239 5.0 µm filter and enumerated using a GUAVA easycyte HT flow cytometer (Millipore). To
240 each agar plate we added ~2000 cells. Cell suspensions were streaked across the agar

241 plates and incubated at 20 ^{o}C until colonies were formed. After 1 month, colonies showing
242 characteristics of *Planctomycetota* (pink pigmentation, budding cell growth) were selected
243 for restreaking. Candidate colonies were restreaked three times to ensure isolation and
244 then identified using 16S rRNA gene metabarcoding of the V4 region using the SILVA Ref NR
245 SSU r138.1 database. To construct a phylogenetic tree, 48 sequences from the
246 *Plactomycetota* family Pirellulaceae in the SILVA Ref NR SSU r138.1 database were
247 selected for alignment using SINA aligner v1.2.11 [51] along with the partial 16S rRNA
248 sequence from our isolate and one sequence from the family Planctomycetales
249 (CP002546.650169.651656 as an outgroup). A maximum-likelihood tree was constructed
250 using RAxML with the GTRGAMMA model. The best scoring tree was visualized using the
251 iTOL server.

252 We tested the ability of an identified *Planctomycetota* isolate within the family
253 Pirellulaceae to grow on model carbohydrates in batch cultures. We prepared artificial
254 seawater (ASW) as incubation medium (0.42M NaCl, 0.029M Na_2SO_4, 0.01M KCl, 1mM KBr,
255 0.05mM H_3BO_3, 0.07mM NaF,0.05M $MgCl_2$, 0.01M $CaCl_2$, 0.06mM $SrCl_2$, 2.5mM $NaHCO_3$).
256 Medium salinity and pH were adjusted to 33 ppt and 7.5, respectively and then autoclaved.
257 Sterile ASW was amended with 0.1 µm filter sterilized vitamin and trace metal solution
258 (1ml L^{-1}) and inorganic nutrients (10 mg L^{-1} NH_4Cl, 1 mg L^{-1} KH_2PO_4). Triplicate 50 ml
259 incubations were prepared for the following treatments: no amendment, *N*-acetyl
260 glucosamine (NAGA), alginate, and fucoidan. Because commercially available fucoidan is
261 typically contaminated, notably by alginate and polyphenols [52, 53], we used ion
262 exchange chromatography (IEX) to purify fucoidan sourced from giant kelp (Sigma-Aldrich,

263 product #F8065). Purification was performed using a medium-scale IEX setup described by
264 Sichert et al., 2021. The composition of the purified fucoidan was checked by ^{1}H-^{13}C HSQC
265 NMR and HPAEC-PAD (Supplemental Figures 2, 3 & 4). Alginate (Sigma-Aldrich PHR1471)
266 and NAGA (Fisher Scientific ICN100068) were certified to be 88 and 100% pure,
267 respectively. An isolate colony was resuspended in sterile ASW without amended
268 carbohydrates. After gently shaking for 20 minutes, the cell suspension was 5.0 µm filtered
269 and enumerated using a GUAVA easycyte HT flow cytometer (Millipore). Cells were added
270 to incubation vessels at a concentration of ~6.0×10^{4} cells ml^{-1}. For all treatments, triplicate
271 control incubations without cells were sampled to confirm sterility of the incubation media
272 and carbohydrate amendments. Incubations were monitored by cell enumeration for nine
273 days.
274
275 **Results**
276 *Kelp physiological response to seasonal nitrate availability and developmental stage*
277 We observed variations in kelp developmental stage driven by seasonal nitrate
278 availability and age. In both seasons, rapid changes in physiology occurred after kelp
279 blades passed 50 days of age, which we use to demarcate the transition from maturity to
280 senescence. Across all samples, tissue-N ($g_{Nitrogen}/g_{Dry\ Weight}$ *100) ranged from 0.63% to
281 3.7%, respectively. Mature kelp sampled in the spring had a significantly higher tissue-N
282 content than mature summer kelp, due to higher seawater nitrate concentrations (Figure 1,
283 Figure 2A; Welch's t-test: $t = -22.6$, $df = 19.0$, $p < 0.001$). Average tissue-N of mature kelp
284 blades in the summer and spring were 0.92 ± 0.08% and 2.6 ± 0.14%, respectively (Figure

2A). After entering the senescent phase, average tissue-N decreased to 0.7 ± 0.06% and 2.1 ± 0.77% in the summer and spring, respectively (Figure 2A).

Seasonal and developmental stage-driven changes in exudate carbohydrate composition

Hydrolyzable carbohydrates averaged 10.3 ± 4.9% of giant kelp exudate carbon across all incubations, regardless of season or age. We observed a significant difference in the carbohydrate sugar content of kelp exudates between the mature and senescent developmental stages (Figure 2B; PERMANOVA, $R^2 = 0.14$, $p < 0.001$) and between seasons (PERMANOVA, $R^2 = 0.07$, $p = 0.006$). Differences in sugar content between developmental stages were driven by the change in mole% of fucose and mannuronic acid (Figure 2B) which made up, on average, 47% and 34% of the sugars exuded in the mature and senescent phases, respectively. Man-URA had the largest change in mole% of all sugars between the mature (5%) and senescent (34%) phases. In mature kelp blade exudates, the molar percentage of glucosamine increased three-fold from summer to spring, demonstrating the largest seasonal change (Figure 2C).

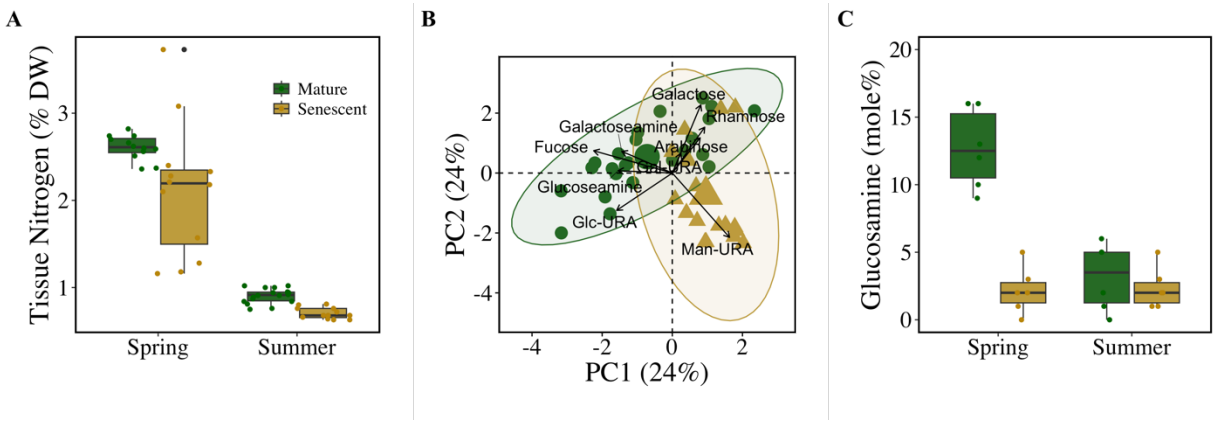

Figure 2. Seasonal and developmental stage changes in giant kelp physiology and exudate carbohydrate composition. **(A)** Giant kelp tissue nitrogen content as a percentage of dry weight (DW) between mature and senescent phase kelp in spring and summer. **(B)**

Principle component (PC) analysis of giant kelp carbohydrate exudates as molar percentages between mature and senescent phase kelp. Ellipses represent 95% confidence regions between mature (green circles) and senescent (gold triangles) kelp exudates. Arrow lengths represent the strength of the correlation between each individual sugar monomer to the two principal components (PC1 & PC2) shown. Large symbols in center of the ellipses are the centroids. Sugar monomer names are overlayed next to arrows. Abbreviations: Glc-URA (glucuronic acid), Gal-URA (galacturonic acid), Man-URA (mannuronic acid). **(C)** Mole% of glucosamine in total moles of sugars exuded by giant kelp between developmental stages and seasons. Green and gold colors represent samples from mature and senescent kelp, respectively and are consistent for all three panels. Boxplots: The top and bottom border of each box represent the 25th and 75th percentiles, the horizontal line inside each box represents the median and the whiskers represent the range of the points (1.5*IQR) excluding outliers. Outliers are shown by black points outside the whiskers. Colored points inside each box are sample values.

Microbe-Carbohydrate dynamics

Coincident with altered exudate carbohydrate composition, we observed significant differences in the giant kelp microbiome between seasons and developmental stages. In both seasons we observed a significant increase in bacterial diversity with age (Ordinary Least Squares regression; Spring: $R^2 = 0.82$, $p < 0.001$; Summer: $R^2 = 0.23$, $p = 0.01$) although the spring cohort had lower initial diversity (Figure 3A). Multivariate analysis demonstrated that the composition of giant kelp microbiome was significantly different between season and developmental stage (Figure 3B; PERMANOVA, $R^2 = 0.10$, $p < 0.001$). Family level shifts between mature and senescent kelp were largely driven by an increase in Flavobacteriacea, Thiotrichaceae, and Arincellaceae and a decrease in Granulosicoccaceae and Pirellulaceae (Figure 4). At the ASV level, we identified 371 taxa that varied significantly in relative abundance between season or developmental stage, most of which were from the phyla *Actinobacteriota, Bacteroidota, Planctomycetota, Proteobacteria* and *Verrucomicrobiota* (FDR adjusted p-values <0.01, DEseq2). Of these

371 ASVs, 44 had a relative abundance > 1% in more than 10% of samples. We consider these 44 ASVs to be abundant and common microbial taxa in the giant kelp microbiome. Hierarchical clustering was used to identify relationships between these 44 abundant ASVs and the mole% of sugars exuded by giant kelp based on Spearman's rank correlation coefficients.

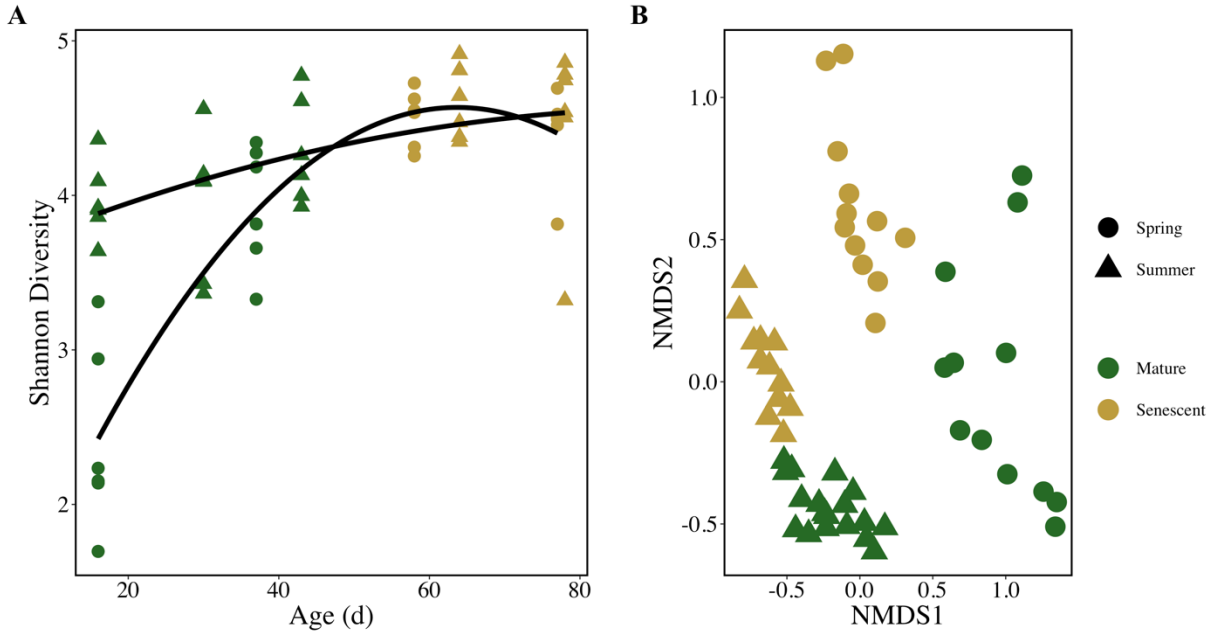

Figure 3. Giant kelp microbiome alpha and beta diversity between seasons and development stage. **(A)** Shannon diversity over age of the blade between spring (circles) and summer (triangles). Solid lines show the significant 2nd order polynomial relationship between giant kelp microbiome Shannon diversity and age. **(B)** NMDS plot showing significant difference in the microbial community composition between seasons and development stage. NMDS ordinations used Bray-Curtis dissimilarities from arcsine-transformed 16s rRNA amplicon relative abundances. The legend applies to both panels.

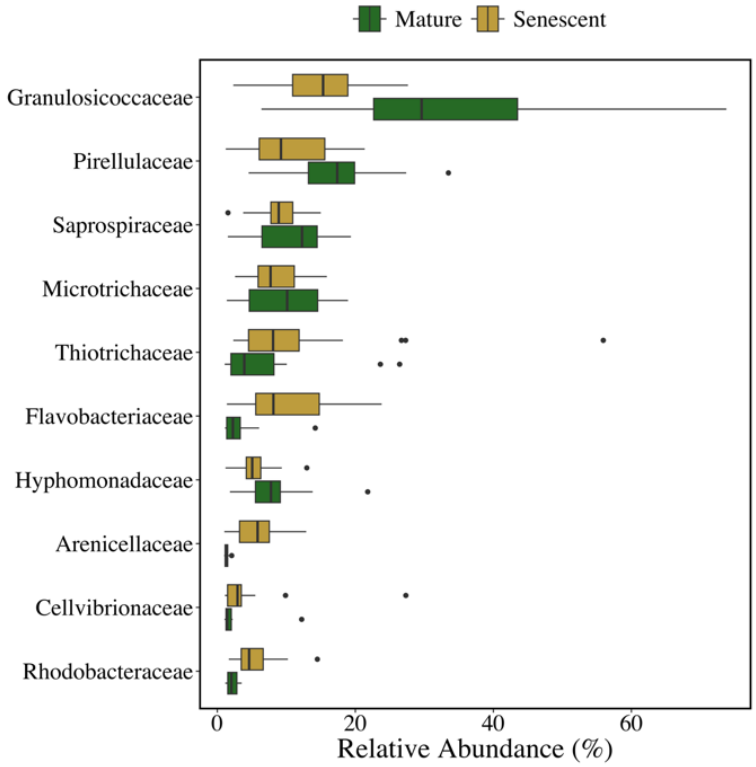

Figure 4. Relative abundance of bacterial clades at the family level on the surface of giant kelp blades between mature and senescent developmental stages. Shown are the top 10 families with a collective relative abundance > 1% during either developmental stage. In each boxplot a point is the relative abundance of a bacterial family in a kelp biofilm sample. The left and right border of each box represent the 25th and 75th percentiles, the vertical line inside each box represents the median and the whiskers represent the range of the points (1.5*IQR) excluding outliers. Outliers are shown by points outside the whiskers.

For 17 of the 44 ASVs there was at least one significant correlation (Spearman's rank correlation, $p < 0.05$, see Supplemental Table 1 & 2) with the mole% of a sugar in giant kelp exudates (Figure 5A). These ASVs grouped into two clusters, primarily based on their correlation with fucose, glucosamine, and mannuronic acid (Figure 5A). The first cluster (Cluster A) included ASVs whose relative abundance was positively correlated with the release of carbohydrates rich in fucose and/or glucosamine or negatively correlated with

367 mannuronic acid (Spearman, $p < 0.05$; see Figure 5A, Supplemental Table 1). Members of
368 the family Pirellulaceae from the phylum Planctomycetota accounted for 3 of the 6 ASVs in
369 Cluster A. Cluster A also contained two ASVs from the genus Granulosicocaceae in the
370 phylum Proteobacteria (Figure 5B).

371 The second cluster (Cluster B) was characterized by a significant positive
372 relationship between ASVs and the release of carbohydrates rich in mannuronic acid
373 (Spearman, $p < 0.05$; see Figure 5A, Supplemental Table 2), and a significant negative
374 correlation with the release of carbohydrates rich in fucose and/or glucosamine
375 (Spearman, $p < 0.05$; see Figure 5A, Supplemental Table 2). This cluster included members
376 of the families Flavobacteriaceae, Cellvibrionaceae, Arenicellaceae, Trueperaceae,
377 Thiotrichaceae and Granulosicoccaceae.

378
379

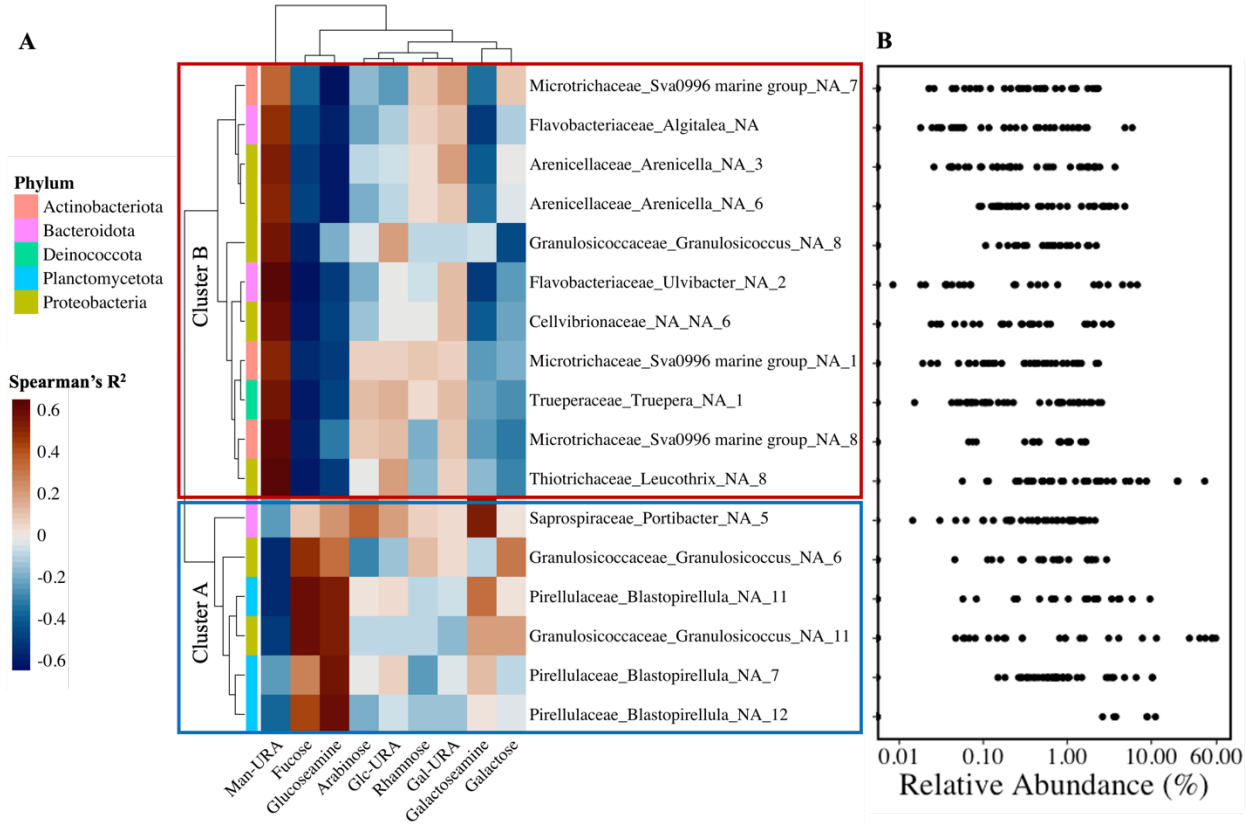

Figure 5. Abundant microbes are differentially correlated to the sugar content of giant kelp exudates. **(A)** Heatmap showing the Spearman's rank correlation coefficient between the relative abundance of differentially abundant ASVs (n = 17) with at least one significant positive or negative correlation with the mole% of a sugar monomer in giant kelp exudates. The strength and direction of the Spearman's ranked correlation are shown by the color ramp. Hierarchical clustering shows two main clusters of ASV-sugar correlations. Cluster A is shown in the blue rectangle, and Cluster B is shown in the red rectangle. The phylum of each ASV is shown by the row color at the tip of each branch. Abbreviations: Glc-URA (glucuronic acid), Gal-URA (galacturonic acid), Man-URA (mannuronic acid). **(B)** Range in the relative abundance of each differentially abundant taxa in all kelp microbiome samples (n = 54).

Planctomycetota growth on model carbohydrates

We cultivated a bacterial isolate from the surface of a giant kelp blade belonging to the phylum *Planctomycetota* (family Pirellulaceae) (Figure 6A & 6B) that we used in subsequent growth assays on model carbohydrates. We confirmed the ability of our

isolate to grow on different carbohydrates, including those from kelp (Figure 6C). We observed no growth in our sterile media controls, or the carbohydrate amended media without cells. In treatments with the *Planctomycetota* isolate added we observed no cell growth in unamended treatments. The isolate grew on both *N*-acetyl glucosamine and fucoidan, but not alginate.

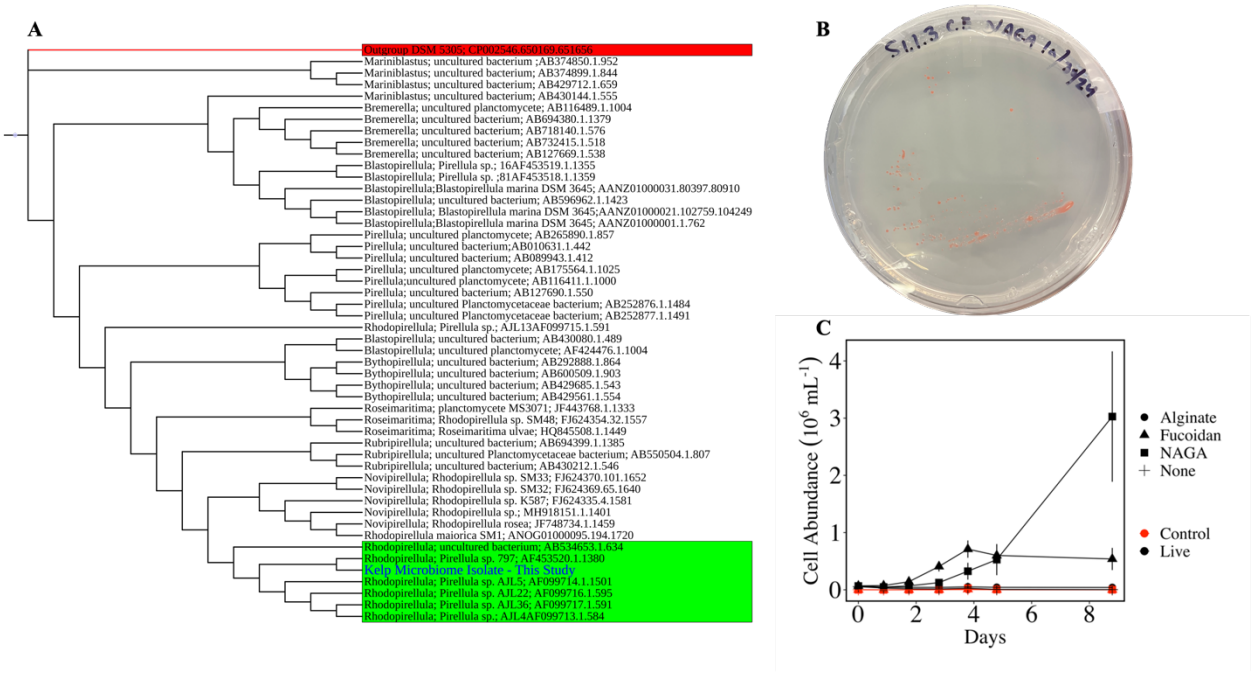

Figure 6. (A) Maximum-likelihood phylogenetic tree of 16s rRNA genes of the Pirellulaceae family. The position of our isolated strain is highlighted in blue text within the Rhodopirellula clade, highlighted by the green box. The tree was rooted with one sequence from the *Planctomycetota* order Planctomycetales, highlighted at the top of the tree. **(B)** Isolation of cultured Rhodopirellula sp. on an agar plate. **(C)** Isolate growth on model carbohydrates. Control incubations (red symbols) are sterile incubation media with all carbohydrate amendments (shapes). NAGA is *N*-acetyl glucosamine. Live incubations (black symbols) show the isolate's growth capability in response to amended carbohydrates. Points and error bars are the mean ±1 standard deviation cell abundance from triplicate incubations.

Discussion

Nutrient availability and age shape kelp physiology

Giant kelp physiology between and within cohorts responded to seasonal nitrogen availability and age-related senescence. At our study site, giant kelp growth is primarily limited by inorganic nitrogen availability, which is depleted in the summer, but is replenished in the spring due to coastal upwelling (Figure 1) [54, 55]. Giant kelp adjusts to periods of low nitrogen availability by adjusting its tissue nitrogen content, resulting in elevated tissue C:N ratios [54] . In our study, the average percent tissue-N of mature giant kelp in the summer (0.91 ± 0.06%) was below the minimum value (0.98%) recorded in the SBC-LTER time-series of kelp at our study site, whereas the percent tissue-N in the spring was, on average (2.6 ± 0.14%), equal to the average for our study site (2.7 ± 0.8%) [55] .In this context, our summer sampling captured kelp in a period of nitrogen depletion (Tissue-N < 1%) which is suggested to result in diminished growth rates and kelp survival [30].

In addition to seasonal fluctuations in physiology, giant kelp undergoes progressive senescence, a rapid decline in developmental stage in response to age [56]. Our results align with previous studies indicating that senescence occurs independently of environmental conditions and begins when kelp tissue age exceeds approximately 50 days [29]. These age-related physiological changes were associated with a decrease in in tissue-N (Figure 2A) and changes in the composition of dissolved carbohydrates released from giant kelp (Figure 2B & 2C).

Giant kelp microbiome composition

The abundance of major epibiont bacterial families at different stages of kelp development is broadly consistent with observations of kelp microbiomes over tissue age and between healthy and stressed or senescent tissue (Figure 4) [33, 36, 37, 57, 58]. Likewise, the increase in diversity and evenness of the microbiome with age is consistent with previous observations [57]; however, to our knowledge this is the first report of significantly lower Shannon diversity in young kelp in the spring compared to the summer (Figure 3A). It has been proposed that the kelp microbiome is established through environmental acquisition over vertical transmission [59]. Therefore, exudates likely play a major role in the establishment and transformation of the kelp microbiome. Kelps continuously shed and replace tissue year-round [60] and factors that affect exudate composition, such as nitrogen availability, may have consequences for the biofilm composition of new tissue, as has been proposed for terrestrial plant rhizospheres [7].

Exudate and microbiome composition dynamics

Simultaneous changes in the carbohydrate composition of kelp exudates and microbial taxa suggest an important role in exudate composition in shaping the kelp microbiome. These associations further revealed that extrinsic factors, such as nitrogen availability, and intrinsic factors such as development stage regulate the composition of the giant kelp exudates. Notably, we observed an enrichment of glucosamine, a nitrogen-containing sugar, in carbohydrates exuded by mature kelp in the spring compared to the nitrogen-limited kelp in the summer (Figure 1C). A similar pattern has been observed in the root exudates of plants, whereby the addition of inorganic nitrogen results in the enhanced

462 release of nitrogen containing metabolites relative to roots grown under nitrogen-limiting
463 conditions [7]. Baker et al., (2024) found that the release of nitrogen-rich metabolites by
464 plant roots selected for a less diverse and unique microbial community compared to
465 plants grown in nitrogen-limited conditions, a pattern we also observed in the kelp
466 microbiome (Figure 2). Glucosamine is a common sugar in the mucus produced by many
467 organisms, including corals and humans [15, 18, 61], and has been shown to serve an
468 important role in regulating attachment and biofilm formation by bacteria [62, 63].
469 Because exudates are constantly sloughed into the surrounding seawater, they must be
470 replaced to maintain their function in the outer membrane layer. Therefore, the cost of
471 exuding nitrogen containing compounds that must be continuously replaced may be too
472 high to be maintained under nitrogen-deplete conditions experienced by giant kelp in the
473 summer.

474 Fucose was the most abundant sugar in the carbohydrates released by mature
475 giant kelp in both seasons, consistent with previous studies of brown macroalgae [17, 64].
476 The abundance of fucose in brown macroalgal exudates is likely due to the secretion of
477 fucoidan, a large sulfated polysaccharide secreted onto the exterior of the cell membrane
478 and shed as mucilage [42]. Fucoidan lacks nitrogen which may explain its consistent
479 dominance in kelp exudates across a range of tissue-N content. Several studies document
480 the potential defensive properties of fucoidans [52, 62, 65] and its proposed defensive role
481 is supported by its observed recalcitrance to bacterial degradation [66].

482 In both seasons, there was an increase in the mole% of mannuronic acid as kelp
483 blades aged and entered the senescent phase (Figure 1B). Mannuronic acid is an indicator

484 of the macroalgal polysaccharide alginate, which comprises up to half of kelp biomass
485 [67]. Microbial taxa positively correlated to the mole% of mannuronic acid included
486 members of the family Flavobacteriaceae and several Gammaproteobacteria, including
487 one member of the family Thiotrichaceae (Figure 4A, Cluster B). Flavobacteria are
488 archetypal fast-growing carbohydrate degraders with adaptations to grow attached to
489 surfaces and utilize high molecular weight organic matter [68, 69]. Using DNA stable
490 isotope probing with ^{13}C-labeled alginate, Thomas et al., (2021) demonstrated the main
491 consumers of alginate in coastal seawater were bacteria from the Flavobacteria,
492 Alteromonas, Thiotrichaceae clades. The relative abundance of Flavobacteria and
493 Thiotrichaceae in kelp biofilms is typically higher on stressed or senescent kelp tissue [58]
494 as observed in this study (Figure 4), and in the early stages of kelp biomass decay these
495 groups dominate alginate hydrolysis [71]. From our observations, we hypothesize that as
496 kelp begins to senesce, the shedding of alginate-rich material promotes the growth of
497 alginate degraders whose hydrolytic enzymes solubilize kelp tissue into DOC. This
498 dynamic would explain the enhanced solubilization of kelp tissue with age that we
499 observed in a complimentary study [72].
500
501 *Potential mechanisms behind carbohydrate-microbe associations*
502 Without further study of their native composition, we can only speculate about the
503 structure and function of the carbohydrates released by giant kelp. However, the role of
504 carbohydrates secreted to the outer membrane layers of animals and phytoplankton is
505 well established. For example, in bacterial biofilm formation, carbohydrates tethered to

506 the cell surface of a host serve as recognition sites for carbohydrate-protein binding
507 proteins (lectins) that act in concert with larger attachment proteins (adhesins). These
508 lectin-adhesin complexes mediate the attachment of bacteria, including pathogens to the
509 host surface [73]. In a model bacterium-diatom association, the lectin *Mp*PA14 exhibits a
510 strong binding affinity for fucose and *N*-acetyl glucosamine residues [62]. Guo et al., (2021)
511 demonstrated that *Mp*PA14 and the *Mp*PA14 lectin homolog from *Vibrio cholera* were
512 inhibited and unable to bind to diatom cells when exposed to high concentrations of free
513 fucose. A strong binding affinity of *Mp*PA14 was also observed for fucoidan, a fucose-rich
514 polysaccharide released by brown macroalgae [42]. These data indicate a potentially
515 conserved defensive role of fucose-containing carbohydrates exuded by members of the
516 Stramenopile lineage, such as diatoms and kelps. Giant kelp may release high
517 concentrations of fucose-rich carbohydrates to disrupt biofilm formation by potential
518 pathogens. Indeed, all taxa from Cluster B (Figure 4A), which includes several taxa
519 associated with macroalgal tissue degradation, such as Flavobacteria, exhibited a
520 negative correlation with the fucose content of the exuded carbohydrates (Spearman, $p <$
521 0.05; see Supplemental Table 1B).
522 Glucosamine may serve as an important carbon and nitrogen source for the growth
523 of microbes beneficial to giant kelp. In the marine environment, glucosamine is more
524 commonly found in its acetylated form (*N*-acetyl glucosamine) [74]. Our carbohydrate
525 measurements require an acid hydrolysis step, which cleaves the acetyl group resulting in
526 glucosamine. Therefore, our glucosamine measurements reflect the contribution of both
527 *N*-acetyl glucosamine and glucosamine residues. The microbial taxa that positively

528 correlated with glucosamine included members from the family Pirellulaceae within
529 *Planctomycetota*, and the *Granulosicoccaceae* family of *Proteobacteria* (Cluster A, Figure
530 5A, Supplemental Table 1). Cultured strains of *Planctomycetota* such as *Pirellula* sp. strain
531 1 can metabolize *N*-acetyl glucosamine (NAGA) as their sole carbon and nitrogen source
532 [75], and in a comparison of 79 cultured members of *Planctomycetota*, *N*-acetyl
533 glucosamine was found to be the most efficient carbon source for their isolation [50].
534 Moreover, previous work suggests *N*-acetyl glucosamine may trigger biofilm formation by
535 some members of *Planctomycetota,* such as *Rhodopirellua baltica* [76].
536 Planctomycetes are dominant members of healthy macroalgal microbiomes [77–
537 79] and it has been proposed they alter the composition of biofilms through the production
538 of secondary metabolites such as stieleriacines [80, 81]. We demonstrate that
539 Planctomycetes isolated from the surface of giant kelp blades can grow on fucoidan and
540 NAGA, but not alginate (Figure 5). This carbohydrate substrate preference is consistent
541 with our observed correlations between the abundance of members of the
542 *Planctomycetota* family Pirellulaceae in the kelp microbiome and the sugar content of
543 giant kelp exudates (Figure 5A, Cluster A). Several recent studies also confirm that the
544 Pirellulaceae family within the *Planctomycetota* phylum specialize in the degradation of
545 fucoidan [71, 80, 82]. Further, metagenome assembled genomes from the kelp *Ecklonia*
546 *radiata* microbiome revealed that fucoidan degradation genes are more frequently present
547 than alginate degradation genes in the Pirellulaceae family [59]. We hypothesize that
548 exudation of specific carbohydrates by kelps serves to enrich their microbiome in
549 commensal or beneficial microbes such as *Planctomycetota*. Such carbohydrate-microbe

550 synergy is consistent with observations of plant rhizospheres, corals and the human gut
551 [13, 15, 61, 83, 84].
552
553 **Concluding remarks and perspectives**
554 There is a growing understanding of the role of microbiomes in maintaining
555 organismal health and ecosystem function [85, 86]. Describing relationships between
556 organism physiology, exudate composition and the microbiome community is the first step
557 in uncovering mechanisms that regulate these interactions. We observed significant
558 variability in the composition of dissolved carbohydrates released by giant kelp in
559 response to seasonal nutrient availability and developmental stage, with corresponding
560 shifts in the kelp microbiome. These findings are particularly relevant given proposals for
561 offshore macroalgal afforestation (OFA) associated with carbon dioxide removal
562 approaches and natural product industries [27, 87]. OFA requires farming in deeper,
563 offshore water, where nutrient concentrations are lower than the shallow coastlines where
564 kelp typically grow. This nutrient stress may impair kelp microbiome establishment and
565 composition resulting in disease or tissue degradation as has been observed during
566 periods of temperature, iron, and pH stress [58, 79, 88, 89]. Future work should determine
567 the functional capacity of key members of the kelp microbiome, such members of the
568 phylum *Planctomycetota*. Such work could enable microbiome-targeted interventions that
569 could be used for beneficial outcomes in offshore kelp aquaculture similar to those
570 applied in terrestrial agriculture [90, 91].
571

Acknowledgments

We thank all past and current members of the Santa Barbara Coastal LTER who generated necessary background data for this study. We thank all Carlson lab members, A. Santoro and D. Siegel for their constructive comments and discussion of the data and manuscript. This project was funded by the Department of Energy's Advanced Research Project Agency-Energy through award DE-AR0001559 to CAC, and the National Science Foundation's Santa Barbara Coastal LTER through award number OCE-1831937 to CAC. CJE and MM were additionally supported by the Worster Family Summer Research Fellowship.

Data Availability

DNA sequence data are available in the National Center for Biotechnology Information Sequence Read Archive under PRJNA1256130. R scripts for analysis can be found at https://github.com/chance-english.

References

1. Anthony MA et al. Forest tree growth is linked to mycorrhizal fungal composition and function across Europe. *ISME J* 2022;**16**:1327–1336. https://doi.org/10.1038/s41396-021-01159-7
2. Beijerinck M. Uber oligonitrophile mikroben. *Zentralbl Bakterol Parasitenkd Infekt Hyg Abt II* 1901;**7**:561–582.
3. Burgunter-Delamare B et al. Metabolic Complementarity Between a Brown Alga and Associated Cultivable Bacteria Provide Indications of Beneficial Interactions. *Front Mar Sci* 2020;**7**. https://doi.org/10.3389/fmars.2020.00085
4. Somers E, Vanderleyden J, Srinivasan M. Rhizosphere Bacterial Signalling: A Love Parade Beneath Our Feet. *Crit Rev Microbiol* 2004;**30**:205–240. https://doi.org/10.1080/10408410490468786
5. Bakshani CR et al. Evolutionary conservation of the antimicrobial function of mucus: a first defence against infection. *Npj Biofilms Microbiomes* 2018;**4**:14. https://doi.org/10.1038/s41522-018-0057-2
6. Mannochio-Russo H et al. Microbiomes and metabolomes of dominant coral reef primary producers illustrate a potential role for immunolipids in marine symbioses. *Commun Biol* 2023;**6**:896. https://doi.org/10.1038/s42003-023-05230-1
7. Baker NR et al. Nutrient and moisture limitations reveal keystone metabolites linking rhizosphere metabolomes and microbiomes. *Proc Natl Acad Sci* 2024;**121**:e2303439121. https://doi.org/10.1073/pnas.2303439121

8. Zhalnina K et al. Dynamic root exudate chemistry and microbial substrate preferences drive patterns in rhizosphere microbial community assembly. *Nat Microbiol* 2018;**3**:470–480. https://doi.org/10.1038/s41564-018-0129-3

9. Abdullah MI, Fredriksen S. Production, respiration and exudation of dissolved organic matter by the kelp *Laminaria hyperborea* along the west coast of Norway. *J Mar Biol Assoc U K* 2004;**84**:887–894. https://doi.org/10.1017/S002531540401015Xh

10. Myklestad SM. Dissolved Organic Carbon from Phytoplankton. In: Wangersky PJ (ed.), Marine Chemistry. Berlin/Heidelberg: Springer-Verlag, 2000, 111–148.

11. Davies PS. The role of zooxanthellae in the nutritional energy requirements of Pocillopora eydouxi. *Coral Reefs* 1984;**2**:181–186. https://doi.org/10.1007/BF00263571

12. Fogg GE. The Ecological Significance of Extracellular Products of Phytoplankton Photosynthesis. *Bot Mar* 1983;**26**. https://doi.org/10.1515/botm.1983.26.1.3

13. Sogin EM et al. Sugars dominate the seagrass rhizosphere. *Nat Ecol Evol* 2022;**6**:866–877. https://doi.org/10.1038/s41559-022-01740-z

14. Wild C et al. Coral mucus functions as an energy carrier and particle trap in the reef ecosystem. *Nature* 2004;**428**:66–70. https://doi.org/10.1038/nature02344

15. Lee STM et al. Mucus Sugar Content Shapes the Bacterial Community Structure in Thermally Stressed Acropora muricata. *Front Microbiol* 2016;**7**:371. https://doi.org/10.3389/fmicb.2016.00371

16. Tremblay P et al. Mucus composition and bacterial communities associated with the tissue and skeleton of three scleractinian corals maintained under culture conditions. *J Mar Biol Assoc U K* 2011;**91**:649–657. https://doi.org/10.1017/S002531541000130X
17. Nelson CE et al. Coral and macroalgal exudates vary in neutral sugar composition and differentially enrich reef bacterioplankton lineages. *ISME J* 2013;**7**:962–979. https://doi.org/10.1038/ismej.2012.161
18. Thobor BM et al. Mucus carbohydrate composition correlates with scleractinian coral phylogeny. *Sci Rep* 2024;**14**:14019. https://doi.org/10.1038/s41598-024-64828-5
19. Krumhansl KA et al. Global patterns of kelp forest change over the past half-century. *Proc Natl Acad Sci* 2016;**113**:13785–13790. https://doi.org/10.1073/pnas.1606102113
20. Miller RJ et al. Giant kelp, Macrocystis pyrifera , increases faunal diversity through physical engineering. *Proc R Soc B Biol Sci* 2018;**285**:20172571. https://doi.org/10.1098/rspb.2017.2571
21. Eger AM et al. The value of ecosystem services in global marine kelp forests. *Nat Commun* 2023;**14**:1894. https://doi.org/10.1038/s41467-023-37385-0
22. Filbee-Dexter K et al. Carbon export from seaweed forests to deep ocean sinks. *Nat Geosci* 2024;**17**:552–559. https://doi.org/10.1038/s41561-024-01449-7
23. Krause-Jensen D, Duarte CM. Substantial role of macroalgae in marine carbon sequestration. *Nat Geosci* 2016;**9**:737–742. https://doi.org/10.1038/ngeo2790
24. Smith SV. Marine Macrophytes as a Global Carbon Sink. *Science* 1981;**211**:838–840.

25. Arafeh-Dalmau N et al. Marine heat waves threaten kelp forests. *Science* 2020;**367**:635–635. https://doi.org/10.1126/science.aba5244

26. Fredriksen S et al. Green gravel: a novel restoration tool to combat kelp forest decline. *Sci Rep* 2020;**10**:3983. https://doi.org/10.1038/s41598-020-60553-x

27. Duarte CM, Bruhn A, Krause-Jensen D. A seaweed aquaculture imperative to meet global sustainability targets. *Nat Sustain* 2022;**5**:185–193. https://doi.org/10.1038/s41893-021-00773-9

28. Bell TW et al. Geographical variability in the controls of giant kelp biomass dynamics. *J Biogeogr* 2015;**42**:2010–2021. https://doi.org/10.1111/jbi.12550

29. Bell TW, Siegel DA. Nutrient availability and senescence spatially structure the dynamics of a foundation species. *Proc Natl Acad Sci* 2022;**119**:e2105135118. https://doi.org/10.1073/pnas.2105135118

30. Gerard VA. Growth and utilization of internal nitrogen reserves by the giant kelp Macrocystis pyrifera in a low-nitrogen environment. *Mar Biol* 1982;**66**:27–35. https://doi.org/10.1007/BF00397251

31. North RJ. Life-span of the Fronds of Giant Kelp, Macrocystis pyrifera. *Nature* 1961;**190**:1215–1216. https://doi.org/10.1038/1901215a0

32. Reed DC, Rassweiler A, Arkema KK. Biomass Rather Than Growth Rate Determines Variation in Net Primary Production by Giant Kelp. *Ecology* 2008;**89**:2493–2505. https://doi.org/10.1890/07-1106.1

33. James AK et al. Giant kelp microbiome altered in the presence of epiphytes. *Limnol Oceanogr Lett* 2020;**5**:354–362. https://doi.org/10.1002/lol2.10157

679 34. Michelou VK et al. The Ecology of Microbial Communities Associated with Macrocystis
680 pyrifera. *PLOS ONE* 2013;**8**:e67480. https://doi.org/10.1371/journal.pone.0067480
681 35. Weigel BL, Pfister CA. Successional Dynamics and Seascape-Level Patterns of
682 Microbial Communities on the Canopy-Forming Kelps Nereocystis luetkeana and
683 Macrocystis pyrifera. *Front Microbiol* 2019;**10**.
684 https://doi.org/10.3389/fmicb.2019.00346
685 36. Marzinelli EM et al. Continental-scale variation in seaweed host-associated bacterial
686 communities is a function of host condition, not geography. *Environ Microbiol*
687 2015;**17**:4078–4088. https://doi.org/10.1111/1462-2920.12972
688 37. Qiu Z et al. Future climate change is predicted to affect the microbiome and condition
689 of habitat-forming kelp. *Proc R Soc B Biol Sci* 2019;**286**:20181887.
690 https://doi.org/10.1098/rspb.2018.1887
691 38. Reed DC, Miller RJ. SBC LTER: Reef: Bottom Temperature: Continuous water
692 temperature, ongoing since 2000. 2025. EDI, 2025.
693 39. Snyder JN et al. Sea Surface Temperature Imagery Elucidates Spatiotemporal Nutrient
694 Patterns for Offshore Kelp Aquaculture Siting in the Southern California Bight. *Front*
695 *Mar Sci* 2020;**7**:22. https://doi.org/10.3389/fmars.2020.00022
696 40. Halewood E et al. Determination of dissolved organic carbon and total dissolved
697 nitrogen in seawater using High Temperature Combustion Analysis. *Front Mar Sci*
698 2022;**9**:1061646. https://doi.org/10.3389/fmars.2022.1061646
699 41. Engel A, Händel N. A novel protocol for determining the concentration and
700 composition of sugars in particulate and in high molecular weight dissolved organic

701 matter (HMW-DOM) in seawater. *Mar Chem* 2011;**127**:180–191.
702 https://doi.org/10.1016/j.marchem.2011.09.004
703 42. Buck-Wiese H et al. Fucoid brown algae inject fucoidan carbon into the ocean. *Proc*
704 *Natl Acad Sci* 2023;**120**:e2210561119. https://doi.org/10.1073/pnas.2210561119
705 43. Giovannoni SJ et al. 16S rRNA genes reveal stratified open ocean bacterioplankton
706 populations related to the Green Non-Sulfur bacteria. *Proc Natl Acad Sci*
707 1996;**93**:7979–7984. https://doi.org/10.1073/pnas.93.15.7979
708 44. Apprill A et al. Minor revision to V4 region SSU rRNA 806R gene primer greatly
709 increases detection of SAR11 bacterioplankton. *Aquat Microb Ecol* 2015;**75**:129–137.
710 https://doi.org/10.3354/ame01753
711 45. Callahan BJ et al. DADA2: High-resolution sample inference from Illumina amplicon
712 data. *Nat Methods* 2016;**13**:581–583. https://doi.org/10.1038/nmeth.3869
713 46. Quast C et al. The SILVA ribosomal RNA gene database project: improved data
714 processing and web-based tools. *Nucleic Acids Res* 2012;**41**:D590–D596.
715 https://doi.org/10.1093/nar/gks1219
716 47. McMurdie PJ, Holmes S. Waste Not, Want Not: Why Rarefying Microbiome Data Is
717 Inadmissible. *PLoS Comput Biol* 2014;**10**:e1003531.
718 https://doi.org/10.1371/journal.pcbi.1003531
719 48. Love MI, Huber W, Anders S. Moderated estimation of fold change and dispersion for
720 RNA-seq data with DESeq2. *Genome Biol* 2014;**15**:550.
721 https://doi.org/10.1186/s13059-014-0550-8

722 49. Lage OM, Bondoso J. Bringing Planctomycetes into pure culture. *Front Microbiol*
723 2012;**3**. https://doi.org/10.3389/fmicb.2012.00405
724 50. Wiegand S et al. Cultivation and functional characterization of 79 planctomycetes
725 uncovers their unique biology. *Nat Microbiol* 2020;**5**:126–140.
726 https://doi.org/10.1038/s41564-019-0588-1
727 51. Pruesse E, Peplies J, Glöckner FO. SINA: Accurate high-throughput multiple sequence
728 alignment of ribosomal RNA genes. *Bioinformatics* 2012;**28**:1823–1829.
729 https://doi.org/10.1093/bioinformatics/bts252
730 52. Patankar MS et al. A revised structure for fucoidan may explain some of its biological
731 activities. *J Biol Chem* 1993;**268**:21770–21776. https://doi.org/10.1016/S0021-
732 9258(20)80609-7
733 53. Sichert A et al. Ion-exchange purification and structural characterization of five
734 sulfated fucoidans from brown algae. *Glycobiology* 2021;**31**:352–357.
735 https://doi.org/10.1093/glycob/cwaa064
736 54. Brzezinksi M et al. Multiple Sources and Forms of Nitrogen Sustain Year-Round Kelp
737 Growth on the Inner Continental Shelf of the Santa Barbara Channel. *Oceanography*
738 2013;**26**:114–123. https://doi.org/10.5670/oceanog.2013.53
739 55. Reed DC, Miller RJ. SBC LTER: Reef: Macrocystis pyrifera CHN content (carbon,
740 hydrogen, nitrogen), ongoing since 2002 ver 21. 2025. EDI, 2025.
741 56. Rodriguez GE et al. The importance of progressive senescence in the biomass
742 dynamics of giant kelp (Macrocystis pyrifera). *Ecology* 2013;**94**:1848–1858.
743 https://doi.org/10.1890/12-1340.1

57. Bengtsson MM et al. Bacterial diversity in relation to secondary production and succession on surfaces of the kelp Laminaria hyperborea. *ISME J* 2012;**6**:2188–2198. https://doi.org/10.1038/ismej.2012.67

58. Minich JJ et al. Elevated temperature drives kelp microbiome dysbiosis, while elevated carbon dioxide induces water microbiome disruption. *PLOS ONE* 2018;**13**:e0192772. https://doi.org/10.1371/journal.pone.0192772

59. Song W et al. Contribution of horizontal gene transfer to the functionality of microbial biofilm on a macroalgae. *ISME J* 2021;**15**:807–817. https://doi.org/10.1038/s41396-020-00815-8

60. Mann KH. Seaweeds: Their Productivity and Strategy for Growth. *Science* 1973;**182**:975–981.

61. Bakshani CR et al. Carbohydrate-active enzymes from Akkermansia muciniphila break down mucin O-glycans to completion. *Nat Microbiol* 2025;**10**:585–598. https://doi.org/10.1038/s41564-024-01911-7

62. Guo S et al. Structural Basis of Ligand Selectivity by a Bacterial Adhesin Lectin Involved in Multispecies Biofilm Formation. *mBio* 2021;**12**:e00130-21. https://doi.org/10.1128/mBio.00130-21

63. Sicard J-F et al. N-Acetyl-glucosamine influences the biofilm formation of Escherichia coli. *Gut Pathog* 2018;**10**:26. https://doi.org/10.1186/s13099-018-0252-y

64. Wada S et al. Quantitative and qualitative analyses of dissolved organic matter released from Ecklonia cava Kjellman, in Oura Bay, Shimoda, Izu Peninsula, Japan. *J Exp Mar Biol Ecol* 2007;**349**:344–358. https://doi.org/10.1016/j.jembe.2007.05.024

766 65. Fitton JH, Stringer DN, Karpiniec SS. Therapies from Fucoidan: An Update. *Mar Drugs*
767 2015;**13**:5920–5946. https://doi.org/10.3390/md13095920
768 66. Sichert A et al. Verrucomicrobia use hundreds of enzymes to digest the algal
769 polysaccharide fucoidan. *Nat Microbiol* 2020;**5**:1026–1039.
770 https://doi.org/10.1038/s41564-020-0720-2
771 67. Kloareg B, Quatrano R. Structure of the cell walls of marine algae and
772 ecophysiological functions of the matrix polysaccharides. *Oceanogr Mar Biol Annu*
773 *Rev* 1988;**26**:259–315.
774 68. Fernández-Gómez B et al. Ecology of marine Bacteroidetes: a comparative genomics
775 approach. *ISME J* 2013;**7**:1026–1037. https://doi.org/10.1038/ismej.2012.169
776 69. Thomas F et al. Characterization of the first alginolytic operons in a marine bacterium:
777 from their emergence in marine Flavobacteriia to their independent transfers to
778 marine Proteobacteria and human gut Bacteroides. *Environ Microbiol* 2012;**14**:2379–
779 2394. https://doi.org/10.1111/j.1462-2920.2012.02751.x
780 70. Thomas F et al. Isotopic tracing reveals single-cell assimilation of a macroalgal
781 polysaccharide by a few marine Flavobacteria and Gammaproteobacteria. *ISME J*
782 2021;**15**:3062–3075. https://doi.org/10.1038/s41396-021-00987-x
783 71. Zhang Y-S et al. Metagenomic insights into the dynamic degradation of brown algal
784 polysaccharides by kelp-associated microbiota. *Appl Environ Microbiol*
785 2024;**90**:e02025-23. https://doi.org/10.1128/aem.02025-23

786 72. English CJ et al. Senescence driven solubilization of biomass is the main source of
787 kelp-derived dissolved organic carbon to the coastal ocean. 2025. EarthArXiv, 2025.
788 https://doi.org/10.31223/X5C71M
789 73. Lewis AL, Kohler JJ, Aebi M. Microbial Lectins: Hemagglutinins, Adhesins, and Toxins.
790 In: Varki A et al. (eds.), Essentials of Glycobiology, 4th ed. Cold Spring Harbor (NY):
791 Cold Spring Harbor Laboratory Press, 2022, 505–516.
792 74. Riemann L, Azam F. Widespread N-Acetyl-d-Glucosamine Uptake among Pelagic
793 Marine Bacteria and Its Ecological Implications. *Appl Environ Microbiol* 2002;**68**:5554–
794 5562. https://doi.org/10.1128/AEM.68.11.5554-5562.2002
795 75. Rabus R et al. Analysis of N-acetylglucosamine metabolism in the marine bacterium
796 Pirellula sp. strain 1 by a proteomic approach. *PROTEOMICS* 2002;**2**:649–655.
797 https://doi.org/10.1002/1615-9861(200206)2:6<649::AID-PROT649>3.0.CO;2-R
798 76. Jeske O et al. Developing Techniques for the Utilization of Planctomycetes As
799 Producers of Bioactive Molecules. *Front Microbiol* 2016;**7**:1242.
800 https://doi.org/10.3389/fmicb.2016.01242
801 77. James AK et al. Giant kelp microbiome altered in the presence of epiphytes. *Limnol*
802 *Oceanogr Lett* 2020;**5**:354–362. https://doi.org/10.1002/lol2.10157
803 78. Lage OM, Bondoso J. Planctomycetes and macroalgae, a striking association. *Front*
804 *Microbiol* 2014;**5**. https://doi.org/10.3389/fmicb.2014.00267
805 79. Qiu Z et al. Future climate change is predicted to affect the microbiome and condition
806 of habitat-forming kelp. *Proc R Soc B Biol Sci* 2019;**286**:20181887.
807 https://doi.org/10.1098/rspb.2018.1887

808 80. Gao X et al. Adaptive traits of *PLANCTOMYCETOTA* bacteria to thrive in macroalgal
809 habitats and establish mutually beneficial relationship with macroalgae. *Limnol*
810 *Oceanogr Lett* 2024;lol2.10424. https://doi.org/10.1002/lol2.10424
811 81. Kallscheuer N et al. The planctomycete Stieleria maiorica Mal15T employs
812 stieleriacines to alter the species composition in marine biofilms. *Commun Biol*
813 2020;**3**:303. https://doi.org/10.1038/s42003-020-0993-2
814 82. Pérez-Cruz C et al. Mechanisms of recalcitrant fucoidan breakdown in marine
815 Planctomycetota. *Nat Commun* 2024;**15**:10906. https://doi.org/10.1038/s41467-024-
816 55268-w
817 83. Bais HP et al. The role of root exudates in rhizosphere interactions with plants and
818 other organisms. *Annu Rev Plant Biol* 2006;**57**:233–266.
819 https://doi.org/10.1146/annurev.arplant.57.032905.105159
820 84. Sasse J, Martinoia E, Northen T. Feed Your Friends: Do Plant Exudates Shape the Root
821 Microbiome? *Trends Plant Sci* 2018;**23**:25–41.
822 https://doi.org/10.1016/j.tplants.2017.09.003
823 85. Peixoto RS et al. Harnessing the microbiome to prevent global biodiversity loss. *Nat*
824 *Microbiol* 2022;**7**:1726–1735. https://doi.org/10.1038/s41564-022-01173-1
825 86. Peixoto RS et al. Beneficial Microorganisms for Corals (BMC): Proposed Mechanisms
826 for Coral Health and Resilience. *Front Microbiol* 2017;**8**.
827 https://doi.org/10.3389/fmicb.2017.00341

87. Ricart AM et al. Sinking seaweed in the deep ocean for carbon neutrality is ahead of science and beyond the ethics. *Environ Res Lett* 2022. https://doi.org/10.1088/1748-9326/ac82ff

88. Paine ER et al. Iron limitation of kelp growth may prevent ocean afforestation. *Commun Biol* 2023;**6**:1–9. https://doi.org/10.1038/s42003-023-04962-4

89. Molnar NB et al. Warming Seawater Temperature and Nutrient Depletion Alters Microbial Community Composition on a Foundational Canopy Kelp Species. *Environ Microbiol* 2025;**27**:e70077. https://doi.org/10.1111/1462-2920.70077

90. Berg G et al. Microbiome Modulation—Toward a Better Understanding of Plant Microbiome Response to Microbial Inoculants. *Front Microbiol* 2021;**12**:650610. https://doi.org/10.3389/fmicb.2021.650610

91. Lucy M, Reed E, Glick BR. Applications of free living plant growth-promoting rhizobacteria. *Antonie Van Leeuwenhoek* 2004;**86**:1–25. https://doi.org/10.1023/B:ANTO.0000024903.10757.6e

Supplementals

Supplemental Table 1. Spearman's correlation R^2 and p-value for abundant ASVs and sugar mole% in Cluster A (Figure 4A). Red and blue filled cells indicate significant ($p < 0.05$) positive and negative correlations, respectively.

Sugar	Pirellulaceae_Blastopirellula_NA_12	Pirellulaceae_Blastopirellula_NA_7	Granulosicoccaceae_Granulosicoccus_NA_11	Pirellulaceae_Blastopirellula_NA_11	Granulosicoccaceae_Granulosicoccus_NA_6	Saprospiraceae_Portibacter_NA_5
Fucose	0.42,0.00566	0.29,0.06614	0.58,5e-05	0.58,6e-05	0.48,0.00145	0.09,0.55564
Rhamnose	-0.13,0.41308	-0.24,0.12203	-0.08,0.61524	-0.1,0.54875	0.11,0.48404	0.06,0.72827
Galactosamine	0.02,0.89114	0.11,0.5006	0.19,0.23305	0.33,0.03406	-0.08,0.59996	0.52,0.00039
Arabinose	-0.2,0.21373	0,0.97687	-0.08,0.61911	0.01,0.9255	-0.29,0.05808	0.34,0.02826
Glucosamine	0.57,8e-05	0.56,0.00011	0.52,0.00041	0.55,0.00018	0.33,0.03539	0.22,0.16389
Galactose	-0.01,0.93022	-0.09,0.58159	0.2,0.19747	0.03,0.86051	0.32,0.03929	0,0.98291
Gal-URA	-0.14,0.3708	-0.03,0.85561	-0.17,0.28965	-0.06,0.70755	0.03,0.82763	0.04,0.81159
Glc-URA	-0.05,0.7488	0.06,0.68583	-0.1,0.52454	0.04,0.80388	-0.13,0.40849	0.18,0.24223
Man-URA	-0.38,0.0134	-0.25,0.10926	-0.51,0.00061	-0.56,0.00012	-0.56,0.00013	-0.24,0.12139

Supplemental Table 2. Spearman's correlation R^2 and p-value for abundant ASVs and sugar mole% in Cluster B (Figure 5A). Red and blue filled cells indicate significant ($p < 0.05$) positive and negative correlations, respectively.

Sugar	Thiotrichaceae_Leucothrix_NA_8	Microtrichaceae_Sva0996 marine group_NA_8	Trueperaceae_Truepera_NA_1	Microtrichaceae_Sva0996 marine group_NA_1	Cellvibrionaceae_NA_NA_6	Flavobacteriaceae_Ulvibacter_NA_2	Granulosicoccaceae_Granulosicoccus_NA_8	Arenicellaceae_Arenicella_NA_6	Arenicellaceae_Arenicella_NA_3	Flavobacteriaceae_Algitalea_NA	Microtrichaceae_Sva0996 marine group_NA_7
Fucose	-0.6, 2e-05	-0.58, 5e-05	-0.62, 1e-05	-0.57, 1e-04	-0.61, 2e-05	-0.65,0	-0.57, 8e-05	-0.48, 0.0014	-0.51, 0.0005	-0.44, 0.0035	-0.38, 0.0127
Rhamnose	-0.16, 0.3242	-0.18, 0.2521	0.04, 0.8013	0.08, 0.6032	-0.01, 0.9413	-0.06, 0.7037	-0.09, 0.5770	0.04, 0.7993	0.04, 0.7804	0.07 ,0.6694	0.1, 0.5407
Galactosamine	-0.16, 0.3239	-0.24, 0.1333	-0.22, 0.1710	-0.24, 0.1276	-0.39, 0.0104	-0.5, 0.0007	-0.07, 0.6481	-0.36, 0.0195	-0.39, 0.0102	-0.49 ,0.0009	-0.35, 0.0217
Arabinose	-0.01, 0.9567	0.1, 0.5379	0.11, 0.5052	0.06, 0.6948	-0.15, 0.3484	-0.2, 0.2132	-0.03, 0.8562	-0.21, 0.189	-0.1, 0.5280	-0.23, 0.1501	-0.17, 0.2698
Glucosamine	-0.5,0. 00066	-0.33, 0.0314	-0.48,0 .00116	-0.52, 0.0004	-0.49, 0.0011	-0.49, 0.0008	-0.2, 0.2071	-0.6, 2e-05	-0.6, 2e-05	-0.58, 7e-05	-0.65, <0.001
Galactose	-0.32, 0.0413	-0.33,0 .03393	-0.28, 0.0755	-0.22,0 .16158	-0.24, 0.1193	-0.26, 0.0974	-0.47, 0.0017	-0.05, 0.7526	-0.02, 0.8790	-0.13, 0.4129	0.08, 0.6033
Gal-URA	0.07, 0.6730	0.08, 0.6147	0.11, 0.4736	0.08, 0.6287	0.13, 0.4252	0.12, 0.4653	-0.09, 0.5704	0.1, 0.5313	0.19, 0.2296	0.12, 0.4623	0.19, 0.2168
Glc-URA	0.21, 0.1893	0.13, 0.4253	0.16, 0.3217	0.07,0 .66731	-0.01, 0.9384	-0.01, 0.9513	0.18, 0.2433	-0.08, 0.6061	-0.07, 0.6777	-0.12, 0.4322	-0.24, 0.1309
Man-URA	0.65,0	0.62, 1e-05	0.55,0 .00018	0.5, 0.0007	0.59, 4e-05	0.64,0	0.57, 8e-05	0.51, 0.0006	0.54, 0.0002	0.48, 0.0012	0.35, 0.0217

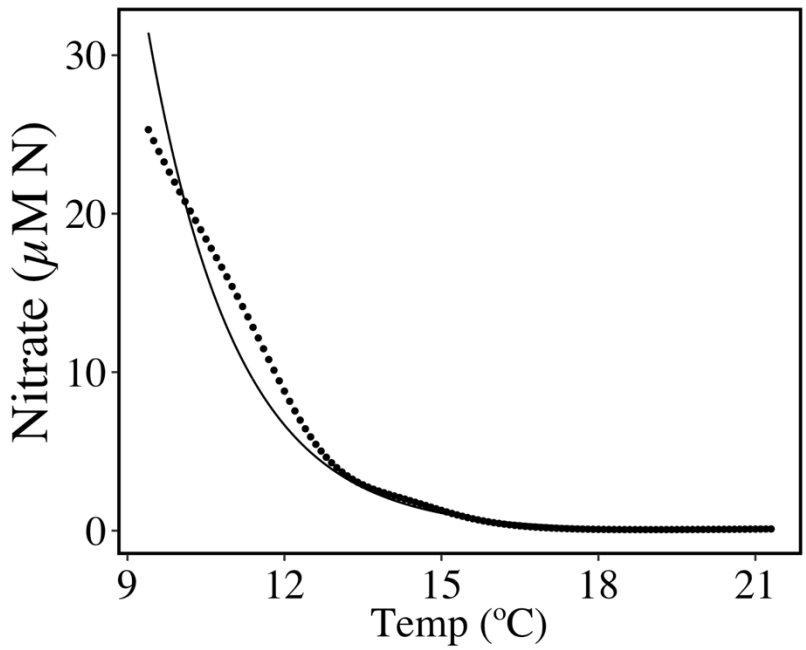

Supplemental Figure 1. Temperature to nitrate relationship for inshore water in the Santa Barbara Channel. Points are from the T2N look up table compiled by Snyder et al. 2020 . Solid line is the exponential regression used to calculate nitrate at Mohawk Reef at our study site: Nitrate (μM N) $= 8565.5 * e^{(-0.597*\text{Temp}(^{o}\text{C}))}$, $R^2 = 0.95$.

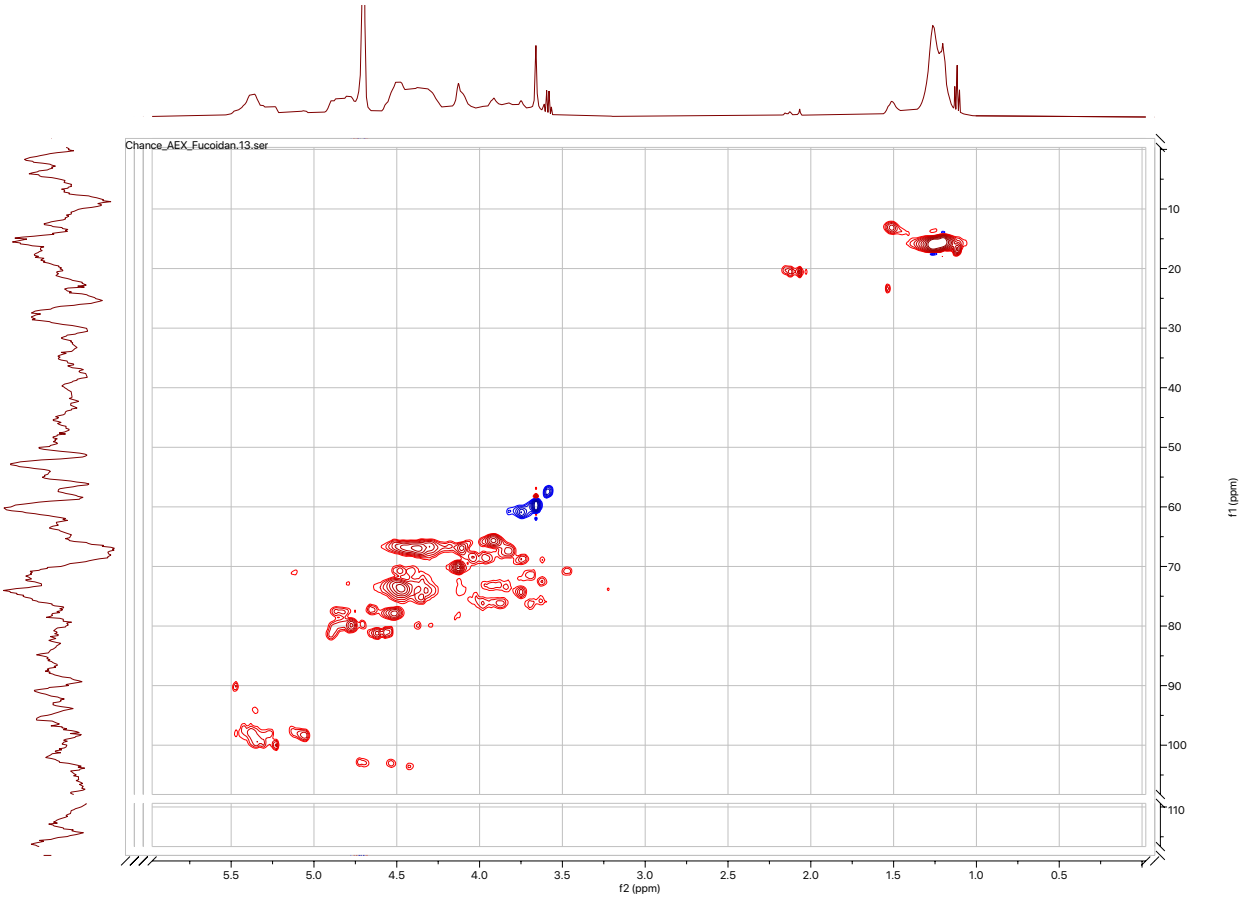

Supplementary Figure 2. ^{1}H-^{13}C HSQC NMR spectrum of IEX purified fucoidan from *Macrocystis pyrifera*. Correlations showing carbons with an even number of protons are blue and those with an odd number of protons are shown in red.

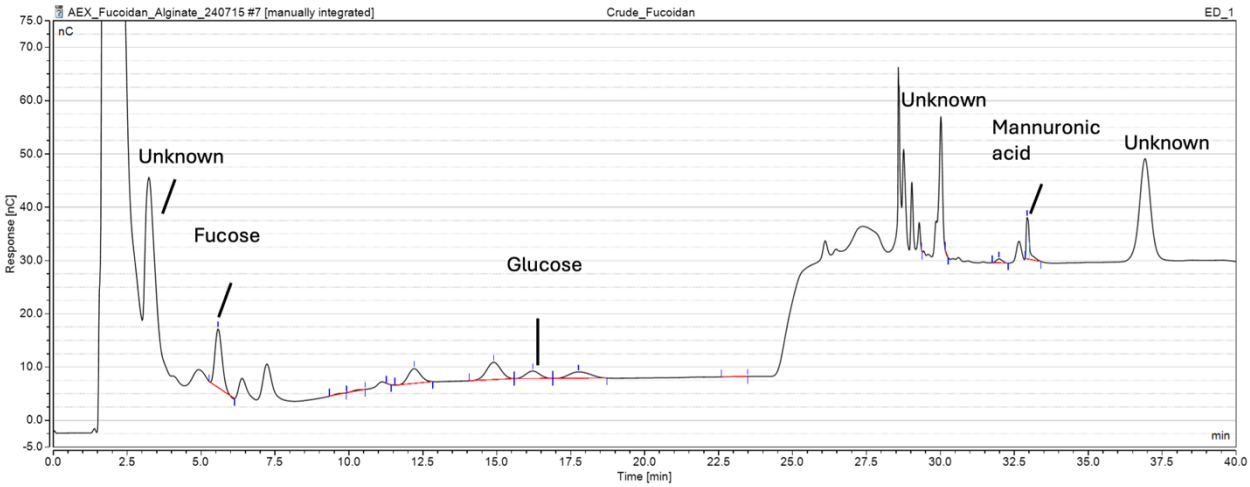

Supplemental Figure 3. HPAEC-PAD chromatogram of crude fucoidan from supplier. Note that peak area for fucose is relatively equal to areas from sugars not found in fucoidan (glucose, mannuronic acid) compared to fucose in IEX-purified fucoidan (Supplemental Figure 4). Also, there are large contributions from unknown peaks, possibly contaminating sugars in the sugar alcohol range (0 - 5 minutes) and acidic sugar range (30 - 40 minutes).

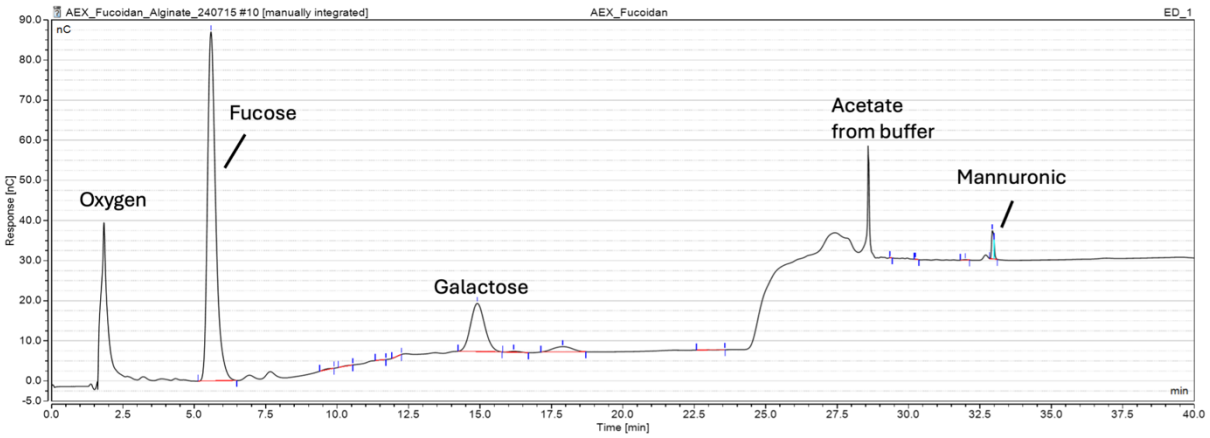

Supplemental Figure 4. HPAEC-PAD chromatogram of IEX purified fucoidan. Note that peak area of fucose enhanced compared to small remaining contaminating sugars (mannuronic acid) compared to Supplemental Figure 3. Contribution of galactose indicates fucoidan from *M. pyrifera* is likely a heterofucan. The two prominent peaks at the beginning and middle of the chromatogram are from dissolved oxygen and acetate from the sample and elution buffer, respectively.